Joint Centre for Mesoscale Meteorology, Reading, UK

The dynamics of a mid-latitude cyclone with very strong latent heat release

Farhang Ahmadi-Givi
George Craig

Internal Report No. 131
NWP Scientific Paper No. 63

July 2001

Met Office

The dynamics of a mid-latitude cyclone with very strong latent heat release

By FARHANG AHMADI-GIVI and GEORGE CRAIG*

University of Reading, UK

SUMMARY

The role of latent heat release in an explosively developing cyclone from the Fronts and Atlantic Storm Track Experiment (FASTEX) has been examined within the potential vorticity (PV) framework. Using conventional synoptic analysis, piecewise PV inversion, and numerical simulations the development has been described in terms of an upper-level PV (UPV) anomaly, a surface potential temperature anomaly and diabatically generated PV anomalies in the lower and upper troposphere. We have attempted to investigate qualitatively and quantitatively the relative contribution of each PV anomaly to the low-level circulation and interactions among them.

In contrast to previous case studies, the results of PV inversion and sensitivity tests reveal that the contribution of the surface thermal anomaly is much weaker than those associated with the upper-level and diabatically generated PV anomalies, which contribute equally to the intensity of the mature cyclone. The low-level PV anomaly is generated rapidly in response to the circulation associated with the UPV anomaly, but its circulation has only a weak effect on upper levels.

However, diabatic reduction of PV in the upper troposphere is found to have two contradictory effects on the UPV anomaly. On the one hand, latent heating tends to destroy the anomaly by inhibiting its downward penetration and reducing its horizontal extent; on the other, it acts to enhance the circulation associated with the anomaly by amplifying the downstream ridge aloft. In magnitude, the negative feedback from latent heating on the UPV anomaly is much stronger than the positive impact, and the low-level circulation associated with the UPV anomaly is substantially decreased by the presence of latent heat release.

KEYWORDS: Cyclogenesis FASTEX Latent heat release Potential vorticity inversion

1. INTRODUCTION

The baroclinic cyclone is the most common phenomenon on synoptic scales in mid-latitudes, and has been a focus of meteorological research for many decades. A great number of theoretical and case studies have specifically investigated the effects of diabatic processes on the baroclinic dynamics (e.g. Danard 1964; Tracton 1973; Gyakum 1983a, b; Emanuel *et al.* 1987; Kuo *et al.* 1991a, b; Davis and Emanuel 1991; Reed *et al.* 1993b; Stoelinga 1996), and it is generally agreed that release of latent heat is the most important among them, particularly in the most sever maritime cyclones.

Theoretical studies (e.g. Emanuel *et al.* 1987, Craig and Cho 1988, Snyder and Lindzen 1991, Montgomery and Farrell 1991, Whitaker and Davis 1994,

* Corresponding author: Department of Meteorology, University of Reading, PO Box 243, Whiteknights, Reading, Berkshire RG6 6BB, UK.

Balasubramanian and Yau 1994, 1996) have consistently shown that latent heat release will increase the growth rates of baroclinic instabilities, while decreasing the horizontal scale of the region of ascent. However the structure of the disturbance remains broadly similar to that of a dry baroclinic instability, unless the magnitude of the latent heat release is very large. In this case, some studies (Craig and Cho 1988, Snyder and Lindzen 1991, and Parker and Thorpe 1995) have found that the diabatic energy conversions can dominate over baroclinic processes, and the structure of the disturbance changes so that it is confined to the region of latent heat release. Apparently, the diabatic heating can provide a dynamical surrogate for the basic state baroclinicity and produce a "moist" baroclinic instability even in situations that are stable in the absence of heating (Snyder and Lindzen 1991, Craig and Cho 1992,). These results suggest that in some cases moist baroclinic instability is not necessarily the result of a cooperative interaction between the diabatic heating and dry baroclinic processes, but rather that the presence of heating introduces distinct effects that may compete with the dry processes. However these linear studies used a highly simplified parameterisation for latent heat release, and the extent to which their results can be applied to the more complex dynamics of real cyclones is unclear.

An attractive approach for investigating the role of latent heat release in observed cyclones is the potential vorticity (PV) framework. As discussed in the seminal paper of Hoskins *et al.* (1985), PV is conserved in the inviscid adiabatic processes of baroclinic instability, while diabatic heating produces sources and sinks of PV. The invertibility principle allows the balanced part of the flow to be obtained uniquely from the PV distribution, along with the potential temperature distribution at the earth's surface.

Using the invertibility principle, a large number of case studies have attempted to quantify the contribution of upper- and lower-level PV anomalies to the low-level cyclone, and to show how these anomalies interact. Their results can be divided into two categories, depending on whether the impact of the diabatically produced PV anomaly on the baroclinic dynamics was very weak or strong. In the weak cases, cyclogenesis is primarily driven by baroclinic dynamics, with latent heat release playing a secondary role (e.g. Hoskins and Berrisford 1988, Davis and Emanuel 1991, Davis *et al.* 1993, Fehlmann and Davis 1998, Huo *et al.* 1999). This situation is shown schematically in Fig. 1, which is adapted from the classic picture of baroclinic instability given by Hoskins *et al.* (1985). The primary effect of latent heat release is to produce a positive PV anomaly in the lower troposphere, located above the surface warm anomaly. The cyclonic circulation associated with the diabatic PV anomaly reinforces that of the surface warm anomaly and enhances the upper-level PV anomaly by advection (Fig. 1b). The growth of the disturbance is enhanced without dramatically changing its structure. Latent heat release also produces a negative PV anomaly in the upper troposphere that can reinforce the upper-level ridge downstream of the cyclone centre, but the effects of this anomaly appear to be less significant (Pomroy and Thorpe 2000).

The validity of this simple picture is, however, questionable when latent heat release makes a very large contribution to the intensity of the surface cyclone, particularly when the surface thermal gradients are weak (e.g. Craig and Cho 1992, Reed *et al.* 1993b, Stoelinga 1996). Indeed, Craig and Cho (1992) hypothesised that the low-level diabatically produced PV anomaly was able to substitute for the absent surface warm anomaly. Instability would occur since the upper-level anomaly would induce ascent that would lead to latent heat release and the intensification of the low-level anomaly. The low-level anomaly would in turn induce a cyclonic circulation that would enhance the upper-level anomaly by advection. In a case study, Stoelinga (1996) found substantial advection of upper-level PV by winds associated with diabatically produced PV in the

lower troposphere. It also seems reasonable to expect that in cases where the diabatic PV production in the lower troposphere is greatest, the diabatic reduction in upper-level PV will also be more significant, however this possibility has received little attention.

In this study we address the question of whether an intense extratropoical cyclone can be produced solely through the interaction of an upper-level PV anomaly with a diabatically produced low-level anomaly as described above. Furthermore we examine how the various PV anomalies interact, in particular, reconsidering the question of whether the negative PV generated in the upper troposphere can have a significant effect in cases where diabatic heating is particularly strong. We do this by investigating a case study, and explosively-developing cyclone from the FASTEX experiment, that showed intense cumulus convection throughout its life-cycle, indicating that latent heat release was likely to have been strong. We investigate the relative contributions of the various upper-level PV, diabatically generated PV, and surface thermal anomalies, and attempt to identify their interactions. The outline of the paper is as follows. Section 2 describes the data and methodology of the study in more detail, whilst section 3 will present a brief synoptic overview of the case. The relative contribution of the anomalies to the low-level circulation is examined in section 4. The results of experiments concerning the interaction between PV anomalies are discussed in section 5. Finally, section 6 will summarise the findings.

2. DATA AND METHODOLOGY

(a) *Data*

This study examined a cyclone from the FASTEX experiment. The FASTEX was an international meteorological field experiment, which took place during January and February 1997. The observing system included a temporally enhanced network of radiosonde stations in Western Europe, seven research aircraft and four ships to provide dropsonde, radiosonde and other observations with high resolution (see Joly *et al.* 1997 and Clough *et al.* 1998 for more information).

The case chosen for study was the subject of an intensive observing period, IOP 18, of the FASTEX. IOP 18 covered the lifecycle of the cyclone, beginning at 0000 UTC 22 February 1997 and ending at 0000 UTC 24 February 1997. The main reasons for choosing this case are: (a) the existence of widespread and intense convection throughout the cyclone development, and (b) its successful forecast by the Met Office limited area model (LAM). The presence of intense convection indicates that condensation, and therefore release of latent heat, is likely to be of great importance to the cyclogenesis. The good control forecast is vital because sensitivity tests using the LAM form an important part of this study. Figure 2 displays three-hourly minimum surface pressure from analysis and control experiment. The analysis data used here is a model-assimilated data (MacPherson *et al.* 1996), which is obtained using the LAM.

(b) *The methodology*

A combination of various approaches is applied to study the IOP18 cyclone. The three components of the methodology are: conventional synoptic analyses, diagnostic analyses of assimilated data using piecewise PV inversion, and analysis of numerical simulations. Applying these approaches, we attempt to identify qualitatively and quantitatively the processes involved in the cyclone development, and in particular the effect of latent heat release. The main characteristics of the PV inversion technique and limited area model used here are described briefly in this section.

(i) *PV inversion.* This study makes extensive use of piecewise PV inversion to attribute aspects of the circulation to particular features in the PV field, allowing the evolution of the flow to be interpreted in terms of interactions between different PV anomalies (Davis and Emanuel 1991, Bishop and Thorpe 1994). The PV inversion system used in this study is described by Griffiths *et al.* (2000). It makes use of the full Ertel-Rossby PV and the Charney (1955) nonlinear balance equation to give the non-divergent wind field associated with the PV distribution. The ability of the PV inversion to reproduce the observed winds depends on the accuracy of the imposed dynamical balance, that is, how closely the balanced winds resemble the observed flow. To evaluate the effect of neglecting irrotational part of winds in the nonlinear balance equation the difference between observed and balanced (nondivergent) winds have been examined, and it was found that the differences are generally small. The largest departures from the calculated balanced flow are about 20% at 850 mb and less than 10% at 400 mb, corresponding to low-level convergence and upper-level divergence near the cyclone centre. This indicates that the analysed wind is adequately captured by the balanced nondivergent wind, thus validating the PV inversion approach.

Here, the layer from 900 mb to 50 mb is used for PV inversion in order to avoid numerical problems due to unstable lapse rates in the planetary boundary layer. In the context of the PV inversion calculations, the term surface potential temperature anomaly will refer to a surrogate anomaly at 900 mb. The lateral boundary conditions used for solving the equations are the same as those used by Davis and Emanuel (1991). On the upper and lower boundaries, Neumann or Dirichlet boundary conditions can be applied. It is found that the wind and temperature fields induced by PV anomalies are almost identical specifying either the wind (Dirichlet) or potential temperature (Neumann) at the horizontal boundaries. Neumann conditions are used for all the calculations shown in this paper.

Contributions of individual PV anomalies to the circulation are determined by performing two successive PV inversions. The first uses the full PV field to find the full balanced wind and potential temperature fields. The second inversion is done on a modified PV field, obtained by subtracting the anomaly from the full PV field. Then the results of the two inversions are subtracted to find the attributed fields induced by the PV anomaly.

It is difficult to construct a universally valid definition of a PV anomaly, which will reliably identify perturbations on strong gradients or those embedded in complex and evolving background fields. Three different methods of anomaly definition have been used in this study, referred to here as the "temporal average", "spatial average", and "objective" methods. In each case the anomaly is defined by first defining a background field where the anomaly has been removed, then subtracting this field from the original one. The temporal average method is perhaps the most commonly used (e.g. Davis and Emanuel 1991, Davis 1992, Stoelinga 1996), and defines the background PV field as the time-averaged PV over the life of the system. The spatial averaging method defines the background field using a spatial average on each vertical level at a single time, and is often useful in the lower troposphere where gradients of PV are small. The objective method removes anomalies by defining a bounding value for PV in a sub-region and resetting higher values (or alternatively lower values) back to the bounding value.

In this study, the upper-level PV (UPV) anomaly is defined using the temporal averaging method. But unlike Davis and Emanuel (1991), we do not use the mean over the whole lifetime of the system. As shown in section 3 the UPV anomaly in our case study appears in the region of high PV values associated with a broad-scale, slowly moving upper trough. Averaging over the life of the cyclone (several days) smoothes out

the broad-scale structure, as well as the localised anomaly associated with the cyclone. A shorter time period (2 days) is therefore used to obtain a mean PV field that retains the broad trough. In particular, the mean state for the present case is defined as the time average between 0000 UTC 22 February and 0000 UTC 24 February 1997.

To define the low-level PV (LPV) anomaly, spatial averaging is used. This is straightforward, as the PV anomaly in the lower troposphere takes the form of an isolated region of diabatically-generated high PV in a background of fairly uniform lower PV values.

To define the surface thermal (θ_B) anomalies, the temporal averaging method is used at earlier times when the warm anomaly is very weak and there are no strong gradients of potential temperature in the vicinity of the cyclone. But at later times both the temporal average and objective methods have been examined. The results of the PV inversion reveal that the temporal average method tends to underestimate the relative contribution of the surface warm anomaly to the low-level circulation. This is because the thermal anomaly defined by temporal averaging contains a cold anomaly along with the warm anomaly associated with the surface cyclone. The intense anti-cyclonic circulation associated with the cold anomaly produces significant cancellation with the circulation induced by the warm anomaly. To isolate the effect of the warm anomaly, the objective method is used to define a background state that omits only the warm temperatures in the vicinity of the surface cyclone.

(ii) *The limited area model.* The Met Office limited area model (LAM), version 4.4, is used in the control experiment and sensitivity tests. It is a part of the Unified Model (Cullen 1993) and is described in detail by Panagi and Dicks (1997). The LAM domain includes Western Europe, the North Atlantic Ocean and the east coast of the United States and Canada. It has a rotated spherical latitude/longitude co-ordinate system with the computational north pole at 30°N, 160°E. This allows even grid spacing at the equator of the rotated grid, which passes roughly through the centre of the domain. The horizontal resolution of the grid is 0.4425 degree in latitude and longitude, which equates to about 50 km over most of the domain. The model is based upon a hybrid σ-pressure co-ordinate with 19 vertical levels. Vertical resolution ranges from 50 m in the first layer to over 2 km in the stratosphere. Boundary conditions for the LAM are obtained from previous global model forecasts.

3. SYNOPTIC OVERVIEW

The evolution of the minimum surface pressure at 3-hourly intervals during IOP 18 is shown in Fig. 2. From the figure it is apparent that there are three stages in the development of the surface cyclone. These are: 1) an incipient stage, where the surface pressure is falling only slowly, 2) an intensification stage where the pressure drops by 33 mb in 21 hrs, and 3) a mature stage where again the pressure falls slowly.

The incipient stage is illustrated by the infrared satellite image for 0000 UTC 22 February, overlaid with contours of surface pressure (Fig. 3a). The incipient cyclone is visible as a small mass of convective cloud over the Labrador Sea (labelled A). This cloud feature is located in a region of positive vorticity advection ahead of an upper-level short wave trough on the upstream side of a major large-scale trough. This can be seen as a region of anomalously low tropopause height (about 2.7 km) in Fig. 4a. A second region of convection in the cold air mass (labelled B) is located further east. The boundaries of the cold air are visible in Fig. 3a as two cloud bands labelled F1and F2.

F1 marks a deep synoptic-scale baroclinic zone with a broad band of moderately deep cloud, and corresponds to the main warm conveyor belt, WCB, in the conceptual model of Harrold (1973). F2 is an old polar front cloud band, which is related to the IOP 17 cyclone.

By 1200 UTC 22 February the cold air feature A has intensified somewhat and moved eastward, whilst a new cloud area (labelled C) is visible between clouds A and B (Fig. 3b). The series of infrared satellite pictures (not shown) reveals the quick growth and rapid east-southeastward motion of this more prominent disturbance (C). The cloud A is not intensified nor increased in size at later times and there is no clear evidence of it at the intensification stage of cyclone. During the incipient stage there is also no apparent interaction between A and F1, and no closed isobar contours at the surface charts. Examination of the fields at 3-hourly intervals indicates that the structure and intensity of the UPV anomaly does not change significantly at the earlier stage. There are no noticeable features related to diabatic PV production in the lower troposphere or thermal advection at the surface during this period.

The first sign of the coming intensification is the appearance of a mid-level cloud extrusion on the cold side of F1 (labelled W2 in Fig. 3b) at 1200 UTC 22 February. This appears as a bulge on F1 at the beginning of the intensification stage but expands and increases in depth (indicated by a higher brightness in the IR images) with time. The band W2 corresponds to the secondary warm conveyor belt, W2, in the conceptual model of Young *et al.* (1987). It is derived from low-level air near the cyclone centre and includes air coming from the lower part of the WCB, which peels off towards the cyclone centre. Bader *et al.* (1995) state that emergence of this cloud is a sign that cyclogenesis is proceeding.

As development continues W2 appears to rotate cyclonically and to approach the cold air feature C. The two cloud features start to merge at 0600 UTC 23 February and to form a comma-head-like shape. Large numbers of convective clouds and thunderstorms exist in the region of the merger at this time (Fig. 3c). Browning (1995) states that the vigorous ascent of the W2 flow typically results in large amounts of precipitation in the region of the cloud extrusion corresponding to the cloud head. Following the merger a significant surface low develops, centred underneath the southern edge of the two cloud masses. By 1200 UTC 23 February the two cloud features are completely indistinguishable on satellite images, as cloud-top temperatures associated with the W2 decrease to values similar to those of the cold air feature. The most rapid deepening of the surface low occurs between 0300 and 0900 UTC 23 February following the cloud mergers (Fig. 2).

Coincident with the emergence of W2 during the intensifying phase, a low-level PV anomaly develops, reaching a value of about 2 PVU (1 PVU = 10^{-6} K kg^{-1} m^2 s^{-1}) at 0600 UTC 23 February (Fig. 5). The region of PV generation coincides with a region where the model analysis indicates significant precipitation, indicating that the PV is diabatically generated by release of latent heat. It is expected that this positive PV anomaly would be accompanied by negative PV production at upper levels (Wernli and Davies 1997, Pomroy and Thorpe 2000) and indeed negative PV values are located downstream of the upper-level trough (see section 5(b)).

The UPV anomaly continues its eastward motion around the base of the large-scale upper trough and begins to rotate cyclonically with time. By 0600 UTC 23 February it is situated on the base of the main trough and achieves a more localised circular shape (Fig. 4b). The magnitude of the PV within the anomaly is somewhat weaker than at earlier times, but its position at the axis of the large-scale trough, combined with the reduction in

PV values in the downstream ridge, lead to a more intense anomaly when compared to its immediate environment.

A small-scale wave, denoting enhanced thermal advection, appears in the low-level potential temperature (θ) charts at 1800 UTC 22 February (not shown). It intensifies with time and reaches its maximum amplitude within 12 hours. Figure 5 shows the θ pattern at 900 mb (solid lines) overlaid with the PV field at 850 mb (dashed lines) for 0600 UTC 23 February. It is noticeable in Fig. 5 that the temperature gradients at the cold and warm front are very weak, about 1 K per 100 km, in comparison with some explosive extratropical cyclones (e.g. Shapiro and Keysor 1990, Davis and Emanuel 1991, Kuo *et al.* 1992, Reed *et al.* 1992). In Kuo *et al.* (1992), for example, a thermal gradient greater than 10 K per 100 km is reported near the low centre during the mature stage.

The mature stage of the IOP18 cyclone is characterised by a wrapping of the cloud band and the dry intrusion, associated with stratospheric PV values, around the low centre. PV anomalies at all levels begin to weaken after achieving their maximum values at the end of the intensification stage.

The synoptic analysis suggests that the pre-existing upper-level PV anomaly plays a key role in initiating cyclogenesis. Both a surface thermal anomaly and low-level diabatically generated PV anomaly are present, and may contribute significantly to the cyclogenesis during the intensifying stage. The relative contribution of each anomaly on the cyclone development will be examined in the next section using PV inversion and numerical experiments.

4. RELATIVE CONTRIBUTION OF PV ANOMALIES

(a) *PV Inversion*

Anomalies of PV in the upper and lower troposphere, and of surface potential temperature have been defined, using the methods described in section 2, every six hours throughout the IOP 18 period. PV inversion is then applied to find out the attributed fields associated with each PV anomaly. A typical example of the piecewise PV inversion results is shown in Fig. 6 for 0600 UTC 23 February, a time when the cyclone is intensifying rapidly. Vertical cross sections are shown for the geopotential-height perturbations associated with each of the three anomalies defined above, as well as the total height perturbation. The UPV anomaly is the dominant contributor at upper levels, but its influence weakens somewhat at lower heights. The LPV and θ_B anomalies are associated with maximum geopotential-height perturbations at low levels that decay rapidly with height. Examples of the horizontal structures of the associated height and wind fields are given by Ahmadi-Givi (2001), but they show little structure since the PV anomalies are not larger than the radius of deformation. The following discussion will characterise the contribution of each anomaly to the cyclone by the associated geopotential-height perturbation at 850 mb. This pressure surface is located within the PV inversion domain, and is close enough to the ground to represent the main features of the surface cyclogenesis. In the example in Fig. 6, the largest contribution is from the UPV anomaly with a significant contribution from the LPV anomaly and a weaker influence associated with the θ_B perturbation.

Figure 7 displays the magnitude of the geopotential-height perturbations at 850 mb associated with each anomaly at every 6 hours for a period beginning at the incipient stage and ending at the mature stage (from 0600 UTC 22 February to 1800 UTC 23 February). In the incipient stage, the UPV anomaly is the dominant contributor to the low-level circulation, while LPV anomaly plays a lesser role and θ_B anomalies are insignificant. In the intensifying stage the 850 mb height-perturbations induced by UPV

and θ_B anomalies amplify slightly with time while the attributed fields induced by the LPV anomaly intensifies greatly. The contribution of the LPV anomaly becomes comparable to the contribution of the UPV anomaly at the end of the intensification phase (1200 UTC 23 February), when latent heat release is a maximum.

An alternative attribution analysis using the quasi-geostrophic omega equation (following Clough and Davitt 1994) has also been carried out. Similar conclusions regarding the contributions of different levels in the atmosphere were found. These diagnostics are described in detail by Ahmadi-Givi (2001).

(b) *Numerical Experiments*

The static PV inversion of the previous section shows the relative importance of each PV anomaly at the specified time, but can give a misleading picture of the relative importance to the cyclogenesis since the anomalies will interact over time. A relatively small circulation associated with a certain PV anomaly may have a crucial role in the development of the cyclone. In this subsection, the PV inversion results are supplemented by numerical experiments where anomalies are removed from the model atmosphere either at a time midway throughout the intensification phase or at the initial time, and the subsequent evolution of the system is followed.

The first set of experiments (described in Table 1) is initialized at a time during the intensifying stage, 0000 UTC 23 February, when all the PV anomalies have developed, and run for 24h. A control experiment with full physics and unmodified initial data (CON1 in Table 1) is performed to provide a standard for comparison. Three sensitivity experiments have been designed to test the impact on the surface cyclogenesis of removing each PV anomaly from the control initial conditions, while keeping all other conditions and model parameters identical to the control simulation. They are referred to as MUP1 (UPV anomaly removed, using temporal averaging), MLP (LPV anomaly removed, using spatial averaging) and MTO (θ_B anomaly removed, using the objective method).

TABLE 1. Experiments initialized at 0000 UTC 23 February and integrated for 24 h

Experiment	UPV anomaly	LPV anomaly	θ_B anomaly	Latent heating	Surface fluxes	Description
CON1	Yes	Yes	Yes	Yes	Yes	Control
MUP1	No	Yes	Yes	Yes	Yes	No UPV anomaly at the initial time
MLP	Yes	No	Yes	Yes	Yes	No LPV anomaly at the initial time
L01	Yes	No	Yes	No	Yes	No latent heat release
LS01	Yes	No	Yes	No	No	No latent heating and surface fluxes
MTO	Yes	Yes	No	Yes	Yes	No θ_B anomaly at the initial time

For the LPV anomaly, another experiment (L01) is performed in which the anomaly is removed from the initial conditions and prevented from redeveloping by setting the latent heat of condensation to zero throughout the experiment. Significant changes to LPV can still occur through surface fluxes, followed by turbulent transport into the troposphere, so a third experiment was made where surface heat fluxes and latent heat release were both removed. Comparable experiments are not possible for UPV and θ_B anomalies that are produced by advection across background gradients, but experiments to define the role of the pre-existing UPV anomaly are described in the next paragraph.

The second set of experiments (described in Table 2) is initialized during the incipient phase of the cyclone development at 0600 UTC 22 February, and integrated for 42h. This period covers the triggering of the cyclone and the main part of its

development. A control simulation (CON2) is carried out and compared to a simulation where the UPV anomaly is removed from the initial conditions (MUP2). Experiments without latent heat release (L02), and without both latent heat and surface heat fluxes (LS02) are also performed. Since there were no significant LPV or θ_B anomalies during the incipient phase, there are no experiments analogous to MLP and MTO (Table 1).

TABLE 2. Experiments initialized at 0600 UTC 22 February and integrated for 42 h

Experiment	UPV anomaly	LPV anomaly	θ_B anomaly	Latent heating	Surface fluxes	Description
CON2	Yes	Yes	Yes	Yes	Yes	Control
MUP2	No	Yes	Yes	Yes	Yes	No UPV anomaly at the initial time
L02	Yes	No	Yes	No	Yes	No latent heat release
LS02	Yes	No	Yes	No	No	No latent heating and surface fluxes

Additional experiments (not shown) have been carried out to test the sensitivity of the results of the MUP1 and MTO experiments to the way in which the PV anomaly is defined. Two experiments were performed with modified initial conditions obtained by removing the UPV by spatial averaging and θ_B anomalies by temporal averaging. The circulations associated with different UPV anomaly definitions were similar, and the subsequent evolution of the simulations was also similar. In the case of the θ_B anomaly, the modified states were noticeably different in structure, but because of the small influence (c.f. Fig. 7) and rapid regeneration of the θ_B anomalies the subsequent development of the cyclone was essentially unchanged.

Figure 8 presents the changes of the minimum surface pressure for the control and other sensitivity experiments listed in Table 1. The simulations support the conclusions of the PV inversion calculations (Fig. 7). In particular, the sensitivity of the cyclogenesis to removal of the θ_B anomaly (MTO) is very small in comparison with the large changes when the UPV anomaly is removed (MUP1) or latent heat is not allowed (L01). Indeed, when latent heating is not allowed throughout the simulation only a weak cyclone is formed. But when the LPV anomaly (mainly due to latent heat release) is removed only at the initial time (MLP), the final pressure of the mature cyclone is not changed significantly. In Fig. 8, the minimum surface pressure in the MLP simulation follows the curve for the no latent heat experiment for about 3 hours, but then intensification resumes and the intensity reached by the MLP cyclone at the end of the experiment is similar to that of the control run. Apparently, the LPV anomaly is regenerated quickly, suggesting that the LPV anomaly of the original cyclone is continually renewed, rather than built up gradually over the life of the cyclone. This feature will be discussed further in the next section. Comparison of the L01 and LS01 experiments also illustrates the very weak impact of surface heat fluxes on the deepening of the surface cyclone.

Figure 8 also shows that when the UPV anomaly is removed (MUP1), surface cyclogenesis is delayed about 9 hours and a weaker cyclone is formed by the end of the simulation. A UPV anomaly is generated in the MUP1 experiment, but it remains much weaker than that of the control experiment (CON1). The generation of this PV anomaly is attributable partly to imperfect isolation of the PV anomaly in the initial conditions and partly to the continued descent and southward advection of stratospheric air. The causes of this advection will be explored in section 5.

The overall pattern seen in the IOP 18 cyclogenesis is quite different from the expected interaction of PV anomalies in baroclinic instability, where the surface cyclone is associated with UPV and θ_B anomalies that intensify as the system develops. Here the

θ_B anomaly appears to play almost no role, the UPV anomaly does not intensify, and the deepening of the surface cyclone is due mainly to the generation of LPV by latent heat release. However, the LPV does not slowly accumulate as the cyclone intensifies, but rather appears to be the results of a process of rapid generation (sufficient to renew the anomaly in 6 hours), presumably accompanied by almost equally rapid destruction. Although growth of the UPV anomaly does not contribute to the cyclogenesis, it appears to play a crucial role in triggering the development.

5. INTERACTION BETWEEN PV ANOMALIES

The conventional picture of baroclinic instability is of UPV and θ_B anomalies acting to reinforce each other by advection across the gradients of the background flow. This interaction is unlikely to describe the IOP18 cyclone, which consisted of a pre-existing UPV anomaly that did not appear to intensify, a diabatically-generated LPV anomaly that increased rapidly, and a consistently weak θ_B perturbation. In this section, the effects of the circulations associated with each PV anomaly on the other anomalies along with the total effect of the LPV anomaly on the UPV anomaly will be examined, to gain a better understanding of why the cyclone intensified in the way that it did. This will be accomplished by applying PV inversion to the model data and performing additional experiments as necessary.

(a) *Influence of UPV anomaly on low-level anomalies*

We first consider the role of the UPV anomaly in generation of the LPV and θ_B anomalies. The numerical experiments of the previous section indicate that the cyclone was triggered by a UPV anomaly that crossed the Labrador coast at 0000 UTC 22 February, so the first question to be addressed is why did surface cyclogenesis begin 15 hours later? Sequences of PV inversion results reveal that the circulation associated with the UPV anomaly does not act to create low-level anomalies at earlier times. Figure 9 shows the circulation induced by the UPV anomaly at 900 mb, overlaid on the potential temperature field on that level, at times before and during the intensification. As can be seen in Fig. 9a, the circulation induced by the UPV anomaly is too far to the north of the low level θ gradient to produce significant advection of warm, moist air. But by 0600 UTC 23 February (Fig. 9b), the UPV anomaly has moved southeastward and approached the region of the theta gradient, drawing a tongue of subtropical air to the north. The role of the UPV anomaly in creating the θ_B perturbation is confirmed in experiment MTO, in which the θ_B anomaly is removed from the control initial conditions. Comparison of the sequences of θ field at 900 mb in MTO and CON1 experiments indicates that the warm anomaly is regenerated quickly and attains magnitudes very close to the control experiment after 6 hours of the simulation. At later times the circulation associated with the growing LPV anomaly also contributes to the warm advaction. Comparison of the θ fields in the L01 and MUP1 experiments suggests that, towards the end of the intensification stage, the UPV and LPV anomalies play comparable roles in generating the thermal anomaly.

In the previous section it was suggested that the LPV anomaly is also regenerated quickly after being removed at the initial time of the MLP experiment. This is seen more clearly on the sequence of PV fields at 850 mb in the MLP simulation. For instance, Fig. 10 illustrates the PV fields in the CON1 and MLP experiments after 12 hours integration. The LPV anomaly was removed from the initial conditions at 0000 UTC 23 February. From Fig. 10b it is evident that the LPV anomaly has intensified quickly, and within 12h attains values slightly less than those of the CON1 experiment (Fig. 10a). In order to

investigate the effect of surface heat fluxes in the generation of the LPV anomaly, the MLP experiment is repeated with the surface fluxes turned off. An examination of the PV field at 850 mb in MLP and new experiments reveals only a 10-15% reduction in the magnitude of the LPV anomaly (not shown). The small role of surface fluxes, and the weak circulations associated with the θ_B anomaly, suggest that the LPV anomaly is formed mainly due to latent heat release in ascending air advected northwards by the UPV anomaly's circulation.

(b) *Influence of LPV anomaly on upper level anomaly*

While it is clear that the UPV anomaly plays the crucial part in developing the lower-level PV anomalies (LPV and θ_B), it is less clear what influence these anomalies have on the UPV anomaly, which does not intensify its contribution to the low-level circulation throughout the life of the cyclone. To look for this influence, the upper-level PV advection by winds induced by LPV and θ_B anomalies is examined. For this purpose the PV field on the 305 K isentropic surface is overlaid with the wind induced by the lower-level anomalies. The sequences of these maps reveal that the feedback from the lower-level PV anomalies on the UPV anomaly is very weak during the incipient phase and increases slightly with time during the intensification stage (not shown).

Figure 11 displays the PV field on the 305 K isentropic surface and upper-level winds due to the LPV and θ_B anomalies at the time of most rapid deepening, 0600 UTC 23 February. Comparison of Figs. 11a and 11b shows that the northerly flows associated with the LPV anomaly are approximately parallel to the PV contours, indicating no significant southward PV advection. On the other hand, the induced southerly winds, which are stronger than northerly winds, may act somewhat to intensify the upper-level ridge immediately downstream of the major trough and slow down the eastward propagation of the UPV anomaly. However, the strength of these circulations is weak, and it appears that the UPV anomaly continues its evolution without substantial advective feedback from the lower-level anomalies.

A second way that latent heat release can influence the upper-level flow is through diabatic modification of the PV field. To detect this influence the control simulation (CON2) can be compared to the run in which latent heat release is not allowed throughout the simulation (L02; see Table 2 for description). Three-hourly time series of minimum surface pressure for each experiment in Table 2 are shown in Fig. 12. As can be seen, in the absence of latent heating (L02), the modelled minimum central is 965 mb compared with 948.7 mb in CON2 experiment. This indicates that latent heat release accounts for a substantial portion of the total deepening. Then PV inversion is applied to the data from L02 experiment for every 6 hours to find out the low-level attributed fields associated with the UPV anomaly excluding latent heat release. These results are also shown in Fig. 7. Because of the weakness of the advective effects of the LPV and θ_B anomalies, any difference in the UPV can be attributed to diabatic modification of the PV field, and indeed comparison of the UPV fields in the two experiments show only localised differences in the regions where condensation is occurring. This simple interpretation would not be possible for most midlatitude cyclones since the removal of latent heat would lead to a changed surface theta distribution, which would give rise to different advective effects at upper-levels, resulting in changes to the PV that are only indirectly related to latent heat release. The surface θ field is changed in experiment LO2, but since it contributes little to the geopotential-height perturbation at 850 mb (Fig. 7), this is of little consequence to the evolution of the cyclone.

A dramatic change in the circulation associated with the UPV anomaly is seen in the experiment where latent heating is removed (Fig. 7). In particular the associated circulation is 30% stronger. In contrast to previous studies, that suggested the existence of a mutual enhancement between the upper-level PV and diabatically produced PV anomalies (e.g. Craig and Cho 1992, Reed *et al.* 1993b, Stoelinga 1996), we find that latent heating has a considerable negative impact on the upper-level PV anomaly. From Fig. 7 it is apparent that this negative feedback increases with time and achieves its maximum at the end of the intensification stage when latent heating is greatest.

To understand how latent heat release influences the UPV anomaly, vertical cross-sections of PV in the CON2 and L02 experiments have been examined. It is found that latent heating acts to inhibit the downward penetration of the UPV anomaly and to decrease the horizontal extent of tropopause fold, as seen for example in Fig. 13, which shows vertical cross-sections of PV for experiments CON2 and L02 at 1200 UTC 23 February. These effects are very weak initially, but increase with time during the intensification stage. The reductions in vertical and horizontal scale of the anomaly will both contribute to decreases in its associated circulation (Hoskins *et al.* 1985). It is worth noting in Fig. 13b the existence of very low PV values, near to zero, covering a broad region at low levels to the east of the tropopause fold. This is associated with near-zero static stability, probably due to dry convective adjustment occurring over a deep layer when latent heat was excluded. This weak low-level static stability may act to enhance the low-level circulation associated with the UPV anomaly, thereby intensifying the cyclone development. However, testing this effect by repeating the PV inversions with tropospheric static stability increased to the values found in the control experiment showed little difference in the strength of the induced circulation.

Comparison of the upper-level PV fields in the CON2 and LO2 experiments also showed a second region of diabatic influence. The small-scale upper-level ridge that forms downstream of the positive UPV anomaly (Fig. 4) as the cyclone intensifies is removed completely in experiment L02, indicating it is created by latent heat release. The effect of this ridge on the low-level attributed fields associated with the UPV anomaly can be determined by using the temporal average method to define a modified PV field, with both the original positive PV anomaly and the negative anomaly of the upper-level ridge removed. A circulation associated with the upper-level ridge-trough combination can then be computed and compared to the circulation calculated previously for the trough alone. The difference in wind perturbations at 850 mb associated with the UPV anomaly including and excluding upper-level ridge for 1200 UTC 23 February is shown in Fig. 14a. From the figure it is evident that the enhancement of the ridge by latent heat release has a positive impact on the cyclonic circulation associated with the UPV anomaly. However, this positive impact must be compared in magnitude to the negative impact of latent heating discussed previously. To do this, Fig. 14b shows the difference in wind perturbations at 850 mb due to the UPV anomaly in the experiments with and without latent heat release (CON2 and L02). Comparison of the two panels in Fig. 14 indicates that the negative influence of latent heat release on the UPV anomaly is much larger than the positive impact generated by intensifying the upper-level ridge. The 850-mb geopotential-height perturbations due to the positive and negative effects of latent heat release on the UPV anomaly are about –8 m and 50 m, respectively.

The various effects of diabatic heating on the UPV anomaly can be summarised with a schematic diagram (Fig. 15). Figure 15a shows the UPV anomaly and its circulation in the absence of latent heating, while Fig. 15b depicts the negative impact of latent heat release on the UPV anomaly by inhibiting its downward penetration and reducing its horizontal extent. Figure 15c provides a qualitative impression of the positive effect of

latent heat release on the UPV anomaly. The upper-level positive PV anomaly and diabatically generated negative PV anomaly on the downstream side of the main trough induce, respectively, cyclonic and anti-cyclonic circulations at the surface (Fig. 15c). The low-level southerly flow associated with the negative PV anomaly is co-located with the southerly flow induced by the positive PV anomaly, thereby leading to enhancement of the effects of the upper-level positive PV anomaly.

(c) Evolution of the UPV anomaly

It was shown earlier that the low-level circulation associated with the UPV anomaly remains at approximately the same strength throughout the cyclone's development (Fig. 7). However, Fig. 7 shows that in the absence of the predominantly negative effects of latent heat release, the geopotential-height perturbation associated with the UPV anomaly intensifies with time. Since the circulation associated with surface θ anomalies are small, whether or not latent heat release is included, the intensification of the UPV anomaly in the absence of latent heating (experiment L02 in Fig. 12) would appear to be due to upper-level processes.

Intensification of synoptic disturbances through upper-level barotropic processes has been examined in a number of recent studies (Cai and Mak 1990, Swanson *et al.* 1997, Kucharski and Thorpe 2000, Lee 2000), and case studies have sometimes shown interaction between upper-level PV anomalies to be important in cyclogenesis (Hakim *et al.* 1996, Huo *et al.* 1999, Chaigne and Arbogast 2000), but it is difficult to identify the precise causes of the amplification of the IOP 18 cyclone. As shown in the synoptic overview, at the initial time the UPV anomaly appears as an elongated anomaly (Fig. 4a) located upstream of the axis of a major upper-level trough. With time, the UPV anomaly moves southeastward around the base of the upper trough. Finally, it is located on the base of the trough and achieves a more localized circular shape at 0600 UTC 23 February (Fig. 4b). Simple superposition of the UPV anomaly with the large-scale PV trough could lead to an enhanced circulation at the surface, but there is also a possibility of nonlinear interactions between them, leading to a localised amplification of the perturbation. Sequences of PV maps on isentropic surfaces reveal that the horizontal deformation increases markedly on the upstream side of the main trough, and the zonal scale of the trough is reduced in the period when the surface cyclone intensifies, which may be associated with a more intense low-level circulation (Hoskins *et al.* 1985).

6. CONCLUSIONS

In this study the role of latent heat release in an explosively developing cyclone has been examined. The goal was to determine whether the dynamics of this case are adequately described by conventional baroclinic instability theory, possibly modified by latent heat effects. This conventional view is summarised from the PV perspective in Fig. 1, where the principle effect of latent heating is seen to be the addition of a positive PV anomaly in the lower troposphere, positioned so as to enhance the effects of the surface thermal anomaly. We examined the IOP 18 cyclone from FASTEX, which appeared to be a system where convection and latent heat release were strong throughout the development of the storm.

In a synoptic analysis, the evolution of the system was divided into three stages. In the incipient stage, a pre-existing upper-level PV (UPV) anomaly was identified, with only a very weak surface thermal perturbation. During the intensification stage, a surface thermal (θ_B) anomaly and low-level PV (LPV) anomaly developed, reaching maximum intensity at the beginning of the mature phase. The magnitude of the UPV anomaly did

not change much as the cyclone intensified. PV inversion diagnostics showed that the contribution of the θ_B anomaly to the deepening of the cyclone is very weak compared with the contributions of the other PV anomalies (Fig. 7). During the intensifying stage, the LPV anomaly amplifies dramatically with time, and eventually contributes as much to the low-level circulation as the UPV anomaly. Numerical experiments in which each of the anomalies were removed showed that the UPV anomaly was crucial for the initiation of the system, the LPV anomaly was responsible for much of the intensity of the cyclone, while the θ_B anomaly was essentially irrelevant (Fig. 8). This lifecycle, consisting of an interaction between UPV and diabatically-generated LPV anomaly is indeed very different from the conventional picture of a mid-latitude cyclone and the remainder of the investigation was devoted to understanding its dynamics.

Sensitivity tests in which the LPV anomaly is removed from the initial conditions revealed that it is regenerated quickly in response to advective forcing from the circulation associated with the UPV anomaly. Surface heat fluxes had only a small effect on the generation of the LPV anomaly. The generation of the θ_B anomaly is attributed equally to the UPV and LPV induced circulations. Examination of PV maps on isentropic surfaces overlaid with winds induced by the LPV and θ_B anomalies indicated only weak advective feedbacks from the lower-level PV anomalies on the upper-level PV anomaly.

The primary effect of latent heat release on the UPV anomaly was through the diabatic decrease of PV at upper levels. Applying PV inversion to the data from an experiment without latent heating throughout the simulation showed that latent heat release has a considerable negative impact on the UPV anomaly, reducing both its downward penetration and its horizontal extent (Figs. 15a, b). This leads to a significant decrease in the low-level winds and height perturbations induced by the UPV anomaly. This result is in contrast to the conclusion of previous studies (e.g. Craig and Cho 1992, Reed *et al.* 1993b, Stoelinga 1996) that there is a mutual enhancement between the UPV and LPV anomalies. An additional product of latent heat release is an upper-level ridge, downstream of the positive UPV anomaly, which has a positive impact on the UPV anomaly by enhancing the southerly flow ahead of it (Fig. 15c). But overall, the negative impact of latent heat release on the UPV anomaly is much larger than the positive effect (Fig. 14). A final aspect of the cyclone, which was not explored in detail, was the amplification of the UPV anomaly in the absence of either latent heating or a significant θ_B anomaly. This may be due to barotropic growth or the interaction of the localised UPV anomaly with the large-scale trough that formed its environment.

The evolution of the IOP 18 cyclone can be summarised as the interaction of a UPV anomaly with a weak low-level baroclinic zone. The low-level thermal gradient was too weak to produce a significant θ_B anomaly, but there was sufficient moisture available to produce a substantial amount of diabatic heating. Diabatic PV production led to a large amplitude LPV anomaly that accounted for much of the growth of the surface cyclone, while weakening the UPV anomaly. This development may be quite different from the conventional picture of mid-latitude cyclogenesis, but it may represent more than an isolated, unusual case. The dominant initial role of the upper-level feature, the persistently weak influence of θ_B anomalies, and the increase of westward tilt with height as the cyclone intensified (here associated with the enhancement of the upper-level downstream ridge) are all characteristics of the "Type C" cyclone introduced by Deveson *et al.* (2000). Using a height-attributable QG vertical motion diagnostic they attempted to generalise the cyclone classification of Petterssen and Smebye (1971). Their objective method was applied to 16 cyclones of the FASTEX. It is shown that 3 cyclones (including the IOP 18 cyclone) do not fit the Type A and Type B categories of Petterssen and Smebye, and these were given the category Type C. Another of these systems is

currently being investigated to see if dynamics are similar to the IOP 18 cyclone analysed here.

ACKNOWLEDGMENTS

The authors wish to thank Dr Morwenna Griffiths for the use of her PV inversion code and Dr Hanna Pomroy for helpful comments concerning PV inversion. Thanks are also to Drs Peter Panagi and Ed Dicks from the Joint Centre for Mesoscale Meteorology at Reading for supplying the limited area model (LAM) data used in this study. F. Ahmadi-Givi is supported by a scholarship from the Iranian Ministry of Science, Research and Technology.

REFERENCES

Ahmadi-Givi, F. 2001 The role of latent heat release in an explosive extratropical cyclogenesis. Ph.D. thesis, Department of Meteorology, University of Reading, 154 pp. [Available from Dept. of Meteorology, University of Reading, Reading, RG6 6BB, UK.]

Bader, M. J., Forbes, G. S., Grant, J. R., Lilley, R. B. E. and Waters, A. J. 1995 Images in weather forecasting. Cambridge University Press, UK

Balasubramanian, G. B. and Yau, M. K. 1994 The effects of convection on a simulated marine cyclone. *J. Atmos. Sci.*, **51**, 2397-2417

Balasubramanian, G. B. and Yau, M. K. 1996 The life cycle of a simulated marine cyclone: energetics and potential vorticity diagnostics. *J. Atmos. Sci.*, **53**, 639-653

Bishop, C. and Thorpe, A. J. 1994 Potential vorticity and the electrostatics analogy: Quasi-geostrophic theory. *Q. J. R. Meteorol. Soc.*, **120**, 713-731

Browning, K. A. 1995 Mesoscale aspects of extratropical cyclones: an observational perspective. Intern. Rep. 44, Joint Centre for Mesoscale Meteorology, Reading, UK

Cai, M. and Mak, M. 1990 On the basic dynamics of regional cyclogenesis. *J. Atmos. Sci.*, **47**, 1417-1442

Chaigne, E. and Arbogast, P. 2000 Multiple potential-vorticity inversions in two FASTEX cyclones. *Q. J. R. Meteorol. Soc.*, **126**, 1711-1734

Charney, J. G. 1955 The use of the primitive equations of motion in numerical prediction. *Tellus*, **7**, 22-26

Clough, S. A. and Davitt, C. S. A. 1994 Development of an Atlantic frontal wave during IOP 3 of fronts 92. Pp. 151-156 in 'The Life Cycles of Extratropical Cyclones', Proceedings of an International Symposium, Geophysical Institute, University of Bergen, 27th June-1st July 1994, (eds. S. GrØnas and M. A. Shapiro) vol. II.

Clough, S. A., Lean, H. W., Roberts, N. M., Birkett, H., Chaboreau, J. P., Dixon, R., Griffiths, M., Hewson, T. D. and Montani, A. 1998 A JCMM overview of FASTEX intensive observing periods. Intern. Rep. 81, Joint Centre for Mesoscale Meteorology, Reading, UK

Craig, G. C. and Cho, H. R. 1988 Cumulus convection and CISK in the extratropical atmosphere. Part I: Polar lows and comma clouds. *J. Atmos. Sci.*, **45**, 2622-2640

Craig, G. C. and Cho, H. R. 1992 Cumulus convection and CISK in midlatitudes. Part II: comma cloud formation in cyclonic shear regions. *J. Atmos. Sci.*, **49**, 1318-1333

Cullen, M. J. P. 1993 The unified forecast/climate model. *Meteorology Mag.*, **122**, 89-94

Danard, M. B. 1964 On the influence of released latent heat on cyclone development. *J. Appl. Meteorol.*, **3**, 27-37

Davis, C. A. 1992 A potential vorticity diagnosis of the importance of initial structure and condensational heating in observed extratropical cyclogenesis. *Mon. Weather Rev.*, **120**, 2409-2428

Davis, C. A. and Emanuel, K. A. 1991 Potential vorticity diagnostics of cyclogenesis. *Mon. Weather Rev.*, **119**, 1929-1953

Davis, C. A., Stoelinga, M. T. and Kuo, Y.-H. 1993 The integrated effect of condensation in numerical simulations of extratropical cyclogenesis. *Mon. Weather Rev.*, **121**, 2309-2330

Deveson, A. C. L., Browning, K. A. and Hewson, T. D. 2000 A classification of FASTEX cyclones using a height-attributable QG vertical motion diagnostic. Intern. Rep. 120, Joint Centre for Mesoscale Meteorology, Reading, UK

Emanuel, K. A., Fantini, M. and Thorpe, A. J. 1987 Baroclinic instability in an environment of small stability to slantwise moist convection. Part I: two-dimensional models. *J. Atmos. Sci.*, 44, 1559-1573

Fehlmann, R. and Davis, H. C. 1998 Role of salient PV-elements in an event of frontal wave cyclogenesis. *Q. J. R. Meteorol. Soc.*, **124**, 1-22

Griffiths, M., Thorpe, A. J. and Browning, K. A. 2000 Convective destabilization by a tropopause fold diagnosed using potential-vorticity inversion. *Q. J. R. Meteorol. Soc.*, **126**, 125-144

Gyakum, J. R. 1983a On the evolution of the QE II storm. I: Synoptic aspects. *Mon. Weather Rev.*, **111**, 1137-1155

Gyakum, J. R. 1983b On the evolution of the QE II storm. II: Dynamic and thermodynamic structure. *Mon. Weather Rev.*, **111**, 1156-1173

Hakim, G. J., Keyser, D. and Bosart, L. F. 1996 The Ohio Valley wave-merger cyclogenesis event of 25-26 January 1978. Part II: Diagnosis using quasigeostrophic potential vorticity inversion. *Mon. Weather Rev.*, **124**, 2176-2205

Harrold, T. W. 1973 Mechanisms influencing the distribution of precipitation within baroclinic disturbances. *Q. J. R. Meteorol. Soc.*, **99**, 232-251

Hoskins, B. J. and Berrisford, P. 1988 A potential vorticity perspective of the storm of 15-16 October 1987. *Weather*, **43**, 122-129

Hoskins, B. J., McIntyre, M. E. and Robertson, A. W. 1985 On the use and significance of isentropic potential vorticity maps. *Q. J. R. Meteorol. Soc.*, **111**, 877-946

Huo, Z., Zhang, D. L. and Gyakum, J. R. 1999 Interaction of potential vorticity anomalies in extratropical cyclogenesis. Part I: Static piecewise inversion. *Mon. Weather Rev.*, **127**, 2546-2561

Joly, A., Jorgensen, D., Shapiro, M. A., Thorpe, A. J., Bessemoulin, P., Browning, K. A., Cammas, J. P., Chalon, J.-P., Clough, S. A., Emanuel, K. A., Eymard, L., Gall, R., Hildebrand, P. H., Langland, R. H., Lemaitre, Y., Lynch, P., Moore, J. A., Persson, P. O. G., Synder, C. and Wakimoto, R. M. 1997 Definition of the fronts and Atlantic Storm-Track Experiment (FASTEX). *Bull. Am. Meteorol. Soc.*, **78**, 1917-1940

Kucharski, F. and Thorpe, A. J. 2000 Upper-level barotropic growth as a precursor to cyclogenesis during FASTEX. Q. J. R. Meteorol. Soc., **126**, 3219-3232

Kuo, Y.–H., Shapiro, M. A. and Donall, E. G. 1991a The interaction of baroclinic and diabatic processes in a numerical simulation of rapidly intensifying extratropical marine cyclone. *Mon. Weather Rev.*, **119**, 368-384

Kuo, Y.–H., Reed, R. J. and Low-Nam, S. 1991b Effects of surface energy fluxes during the early development and rapid intensification stages of seven explosive cyclones in the western Atlantic. *Mon. Weather Rev.*, **119**, 457-476

Kuo, Y.-H., Reed, R. J. and Low-Nam, S. 1992 Thermal structure airflow in a model simulation of an occluded marine cyclone. *Mon. Weather Rev.*, **120**, 2280-2297

Lee, S. 2000 Barotropic effects on atmospheric storm tracks. *J. Atmos. Sci.*, **57**, 1420-1435

Macpherson, B., Wright, B. J., Hand, W. H. and Maycock, A. J. 1996 The impact of MOPS moisture data in the UK Meteorological Office mesoscale data simulation scheme. *Mon. Weather Rev.*, **124**, 1746-1766

Montgomery, M. T. and Farrell, B. F. 1991 Moist surface frontogenesis associated with interior potential vorticity anomalies in a semi-geostrophic model. *J. Atmos. Sci.*, **48**, 343-367

Panagi, P. and Dicks, E. 1997 Met. Office Unified Model, diagnostic, graphics programs, and other observational data available from the JCMM through the aegis of the Universities Weather Research Network (plus Supplement). Intern. Rep. 69, Joint Centre for Mesoscale Meteorology, Reading, UK

Parker, D. J. and Thorpe, A. J. 1995 Conditional convective heating in a baroclinic atmosphere: a model of convective frontogenesis. *J. Atmos. Sci.*, **52**, 1699-1711

Pomroy, H. R. and Thorpe, A. J. 2000 The evolution and dynamical role of reduced upper-tropospheric potential vorticity in intensive observing period one of FASTEX. *Mon. Weather Rev.*, **128**, 1817-1834

Reed, R. J., Stoelinga, M. T. and Kuo, Y.-H. 1992 A model-aided study of the origin and evolution of the anomalously high potential vorticity in the inner region of a rapidly deepening marine cyclone. *Mon. Weather Rev.*, **120**, 893-913

Reed, R. J., Grell, G. A. and Kuo, Y.-H.	1993b	The ERICA IOP5 Storm. Part II: Sensitivity tests and further diagnosis based on model output. *Mon. Weather Rev.*, **121**, 1595-1612
Shapiro, M. A. and Keyser, D.	1990	Fronts, Jet streams and the tropopause. In 'Extratropical Cyclones. The Eric Palmen Memorial Volume'. *Amer. Meteorol. Soc.*, 167-191
Snyder, C. and Lindzen, R.	1991	Quasi-geostrophic wave-CISK in an unbounded baroclinic shear. *J. Atmos. Sci.*, **48**, 76-86
Stoelinga, M. T.	1996	A potential vorticity-based study of the role of diabatic heating and friction in a numerically simulated baroclinic cyclone. *Mon. Weather Rev.*, **121**, 849-874
Swanson, K. L., Kushner, P. J. and Held, I. M.	1997	Dynamics of barotropic storm tracks. *J. Atmos. Sci.*, **54**, 791-810
Tracton, M. S.	1973	The role of cumulus convection in the development of extratropical cyclones. *Mon. Weather Rev.*, **101**, 573-592
Wernli, H. and Davies, H. C.	1997	A lagrangian based analysis of extratropical cyclone. I: The method and some applications. *Q. J. R. Meteorol. Soc.*, **123**, 467-489
Wernli, H. and Davies, H. C.	1997	A lagrangian based analysis of extratropical cyclone. II: A detailed case-study. *Q. J. R. Meteorol. Soc.*, **123**, 1677-1706
Whitaker, J. S. and Davis, C. A.	1994	Cyclogenesis in a saturated environment. *J. Atmos. Sci.*, **51**, 889-907
Young, M. V., Monk, G. A. and Browning, K. A.	1987	Interpretation of satellite imagery of a rapidly deepening cyclone. *Q. J. R. Meteorol. Soc.*, **113**, 1089-1115

List of figures:

Figure 1. (a) schematic illustration of circulations associated with upper-level PV and surface warm anomalies, acting to reinforce each other (Adapted from Hoskins *et al.* 1985); (b) circulation associated with the diabatically produced positive PV anomaly, acting to re-enforce the surface warm anomaly and to enhance advection of upper-level PV.

Figure 2. Time series of central pressure (mb) of the IOP 18 cyclone at 3-h intervals in the control simulation and analysis, during the period 0000 UTC on 22nd to 0000 UTC on 24th February 1997.

Figure 3. Meteosat infrared satellite images of the North Atlantic region overlaid with mean sea-level pressure contours at 4 mb interval for (a) initial time (0000 UTC 22 February), (b) end of the incipient stage (1200 UTC 22 February) and (c) intensification stage (0600 UTC 23 February). Temperature scale of clouds is shown at right of each panel. Letters mark cloud features discussed in text.

Figure 4. Height of the 2 PVU surface for (a) 0000 UTC 22 February and (b) 0600 UTC 23 February 1997. Height scale is shown at right of each panel.

Figure 5. Potential temperature at 900 mb (solid lines, 4 K contour interval) overlaid with PV field (dashed lines, 0.5 PVU in contour interval) at 850 mb for 0600 UTC 23 February 1997.

Figure 6. X-Z cross-sections of geopotential-height perturbations associated with PV anomalies at 0600 UTC 23 February: (a) UPV, (b) LPV, (c) θ_B anomaly, and (d) total effect of PV anomalies. Cross-sections in Figs. (a) - (d) correspond to 44.5-53°N and 3.5-61°W. Contour interval in panels (a) and (b) is 2 dam and in panel (c) is 1 dam, with negative values dashed.

Figure 7. The contributions to the 850-mb geopotential-height perturbation from upper-level PV anomaly (UPV), diabatically produced PV anomaly (LPV), surface thermal anomaly (Theta), and upper-level PV anomaly in experiment L02, without latent heat release (UPV(L02)). Time period starts at 0600 UTC 22 February and ends at 0000 UTC 24 February 1997.

Figure 8. Three-hourly time series of central pressure (mb) from control and sensitivity tests. See Table 1 and text for explanation of abbreviations.

Figure 9. Winds at 900 mb induced by the UPV anomaly (vectors) overlaid with potential temperature on that level (solid lines, 3 K contour interval) for (a) 0600 UTC 22 February and (b) 0600 UTC 23 February 1997.

Figure 10. 850-mb PV (contour interval 0.5 PVU) for (a) CON1 and (b) MLP experiments at 1200 UTC 23 February, 12h after the start of the integration.

Figure 11. PV field on the 305 K isentropic surface at 0600 UTC 23 February with wind vectors overlaid: (a) original winds, (b) winds induced by the LPV anomaly, and (c) winds induced by the θ_B anomaly. PV contour interval is 1 unit, with values between 2 and 3 shaded. Note the different wind vector scales at upper right.

Figure 12. Three-hourly time series of central pressure (mb) from control and sensitivity experiments. See Table 2 and text for explanation of abbreviations.

Figure 13. North – south cross sections of PV at 1200 UTC 23 February 1997; (a) CON2 and (b) L02 experiments. Contour interval is 0.5 PVU.

Figure 14. Change in 850-mb winds associated with UPV anomaly at 1200 UTC 23 February when (a) downstream ridge aloft excluded, and (b) all effects of latent heat release excluded. Vector scales in m s^{-1} are shown at upper right.

Figure 15. Schematic illustration of the various effects of latent heat release on the low-level circulation associated with the UPV anomaly; (a) with no latent heat release, (b) the negative effect, and (c) the positive effect. See text for explanation.

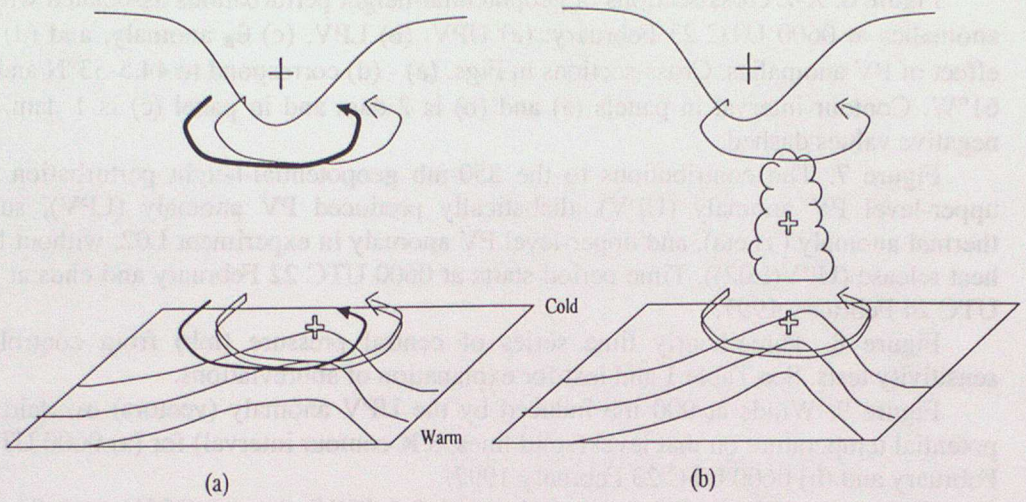

Figure 1. (a) Schematic illustration of circulations associated with upper-level PV and surface warm anomalies, acting to reinforce each other (Adapted from Hoskins *et al.* 1985); (b) circulation associated with the diabatically produced positive PV anomaly, acting to re-enforce the surface warm anomaly and to enhance advection of upper-level PV.

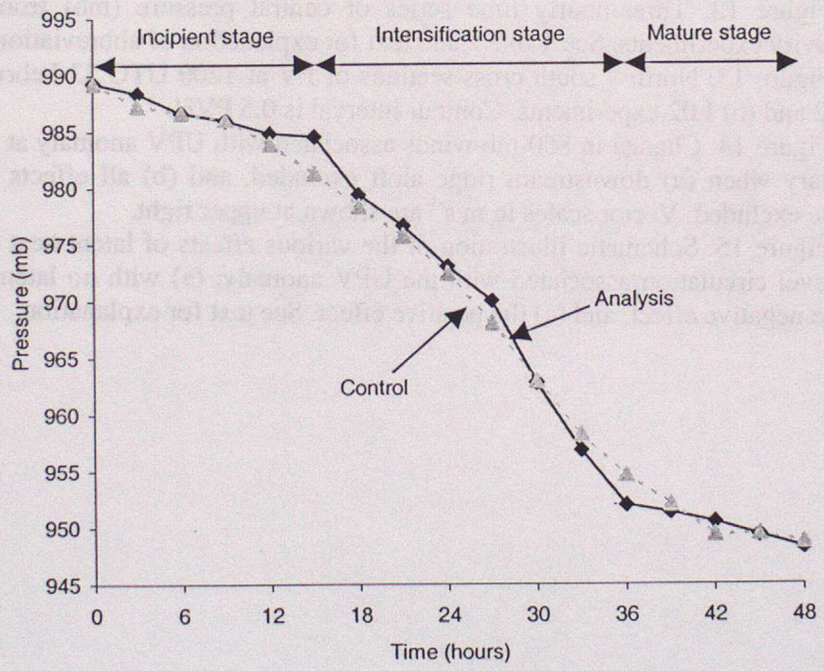

Figure 2. Time series of central pressure (mb) of the IOP 18 cyclone at 3-h intervals in the control simulation and analysis, during the period 0000 UTC on 22nd to 0000 UTC on 24th February 1997.

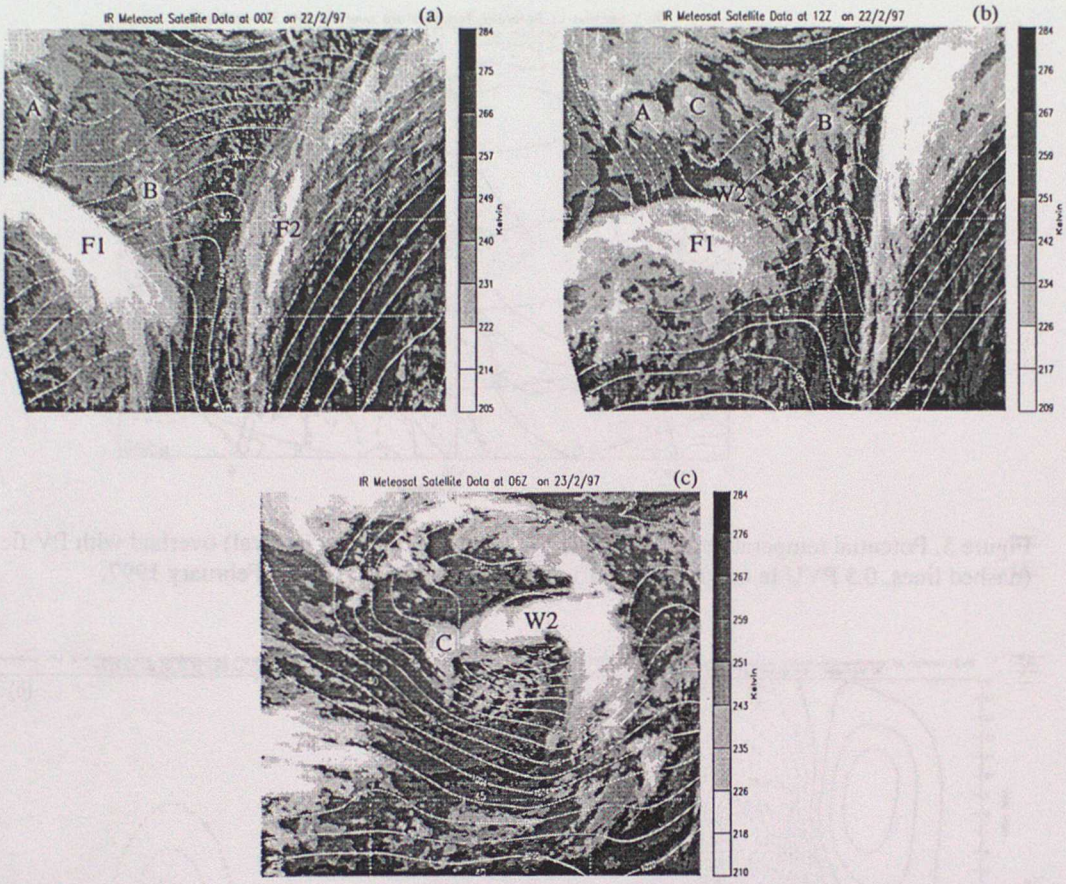

Figure 3. Meteosat infrared satellite images of the North Atlantic region overlaid with mean sea-level pressure contours at 4 mb interval for (a) initial time (0000 UTC 22 February), (b) end of the incipient stage (1200 UTC 22 February) and (c) intensification stage (0600 UTC 23 February). Temperature scale of clouds is shown at right of each panel. Letters mark cloud features discussed in text.

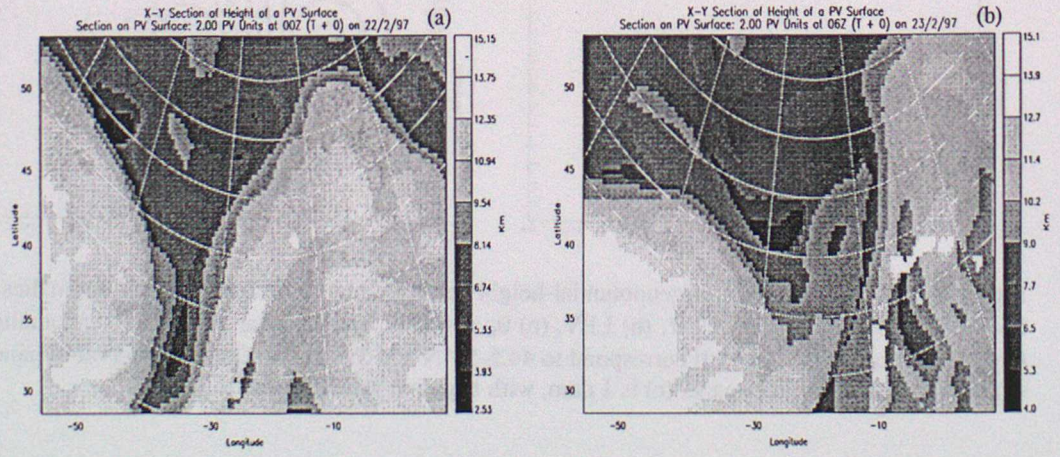

Figure 4. Height of the 2 PVU surface for (a) 0000 UTC 22 February and (b) 0600 UTC 23 February 1997. Height scale is shown at right of each panel.

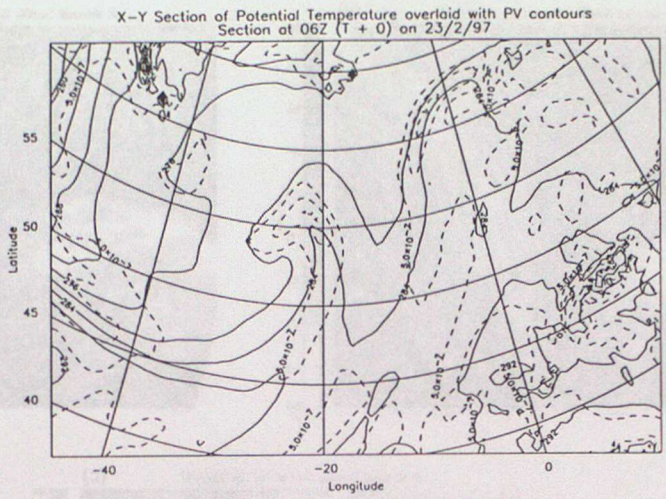

Figure 5. Potential temperature at 900 mb (solid lines, 4 K contour interval) overlaid with PV field (dashed lines, 0.5 PVU in contour interval) at 850 mb for 0600 UTC 23 February 1997.

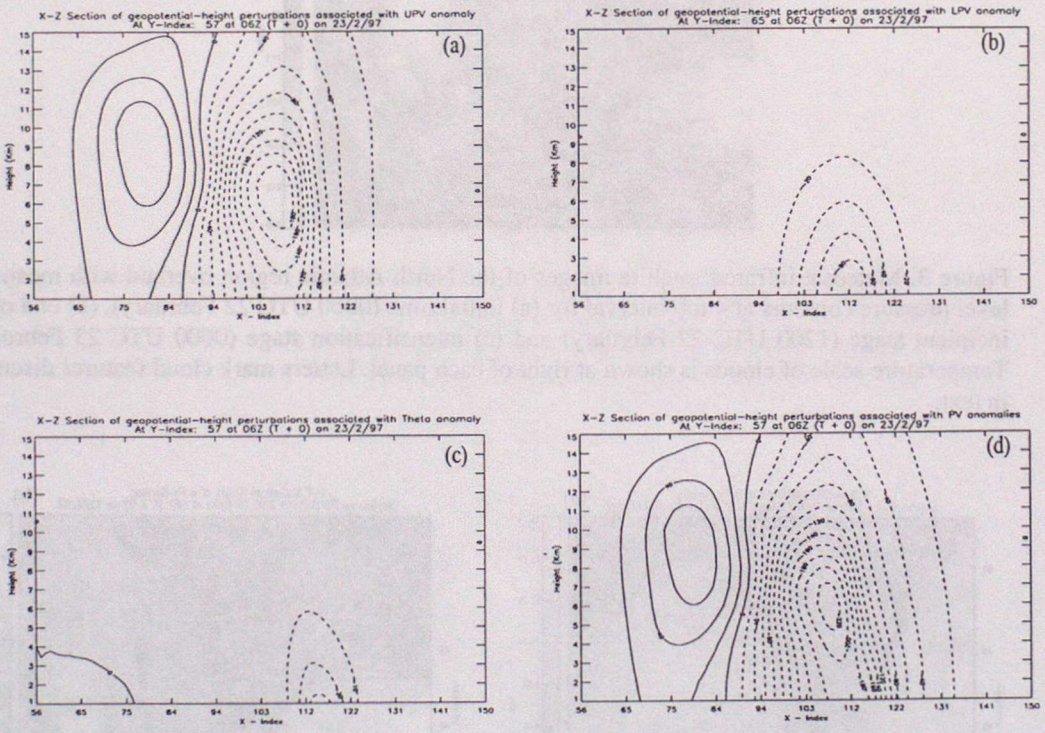

Figure 6. X-Z cross-sections of geopotential-height perturbations associated with PV anomalies at 0600 UTC 23 February: (a) UPV, (b) LPV, (c) θ_B anomaly, and (d) total effect of PV anomalies. Cross-sections in Figs. (a) - (d) correspond to 44.5-53°N and 3.5-61°W. Contour interval in panels (a) and (b) is 2 dam and in panel (c) is 1 dam, with negative values dashed.

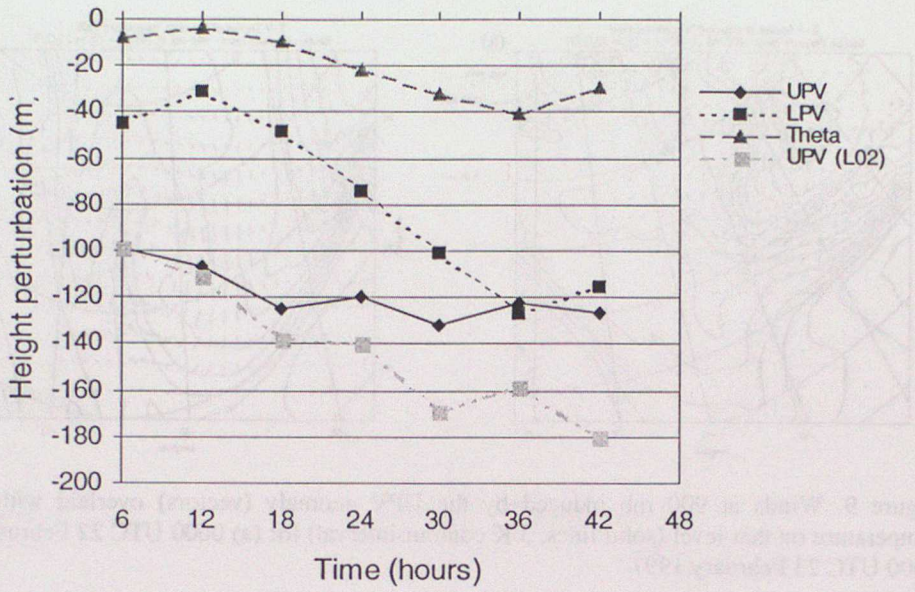

Figure 7. The contributions to the 850-mb geopotential-height perturbation from upper-level PV anomaly (UPV), diabatically produced PV anomaly (LPV), surface thermal anomaly (Theta), and upper-level PV anomaly in experiment L02, without latent heat release (UPV(L02)). Time period starts at 0600 UTC 22 February and ends at 0000 UTC 24 February 1997.

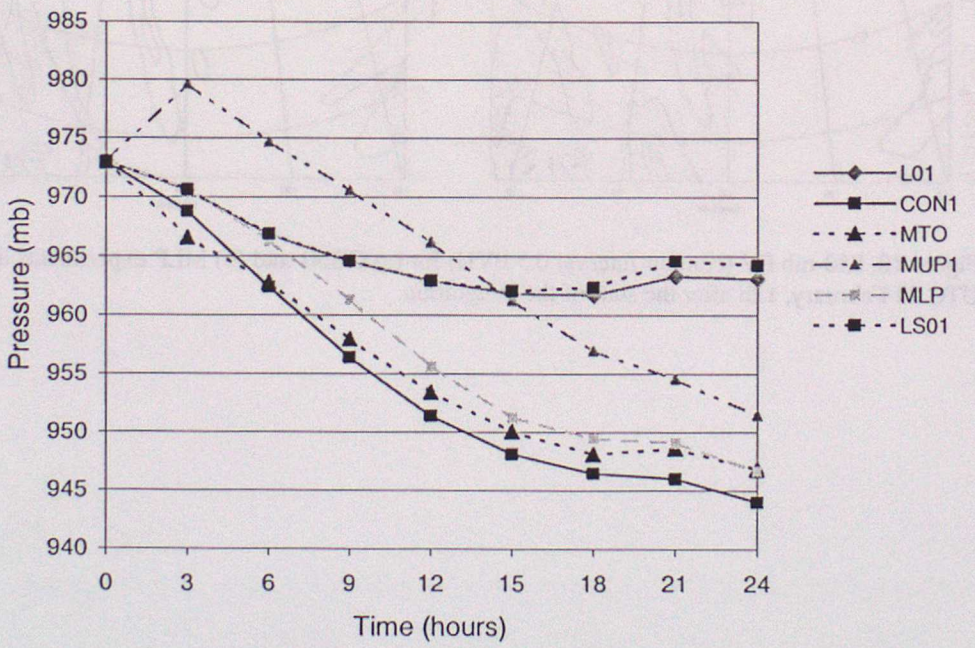

Figure 8. Three-hourly time series of central pressure (mb) from control and sensitivity tests. SeeTable 1 and text for explanation of abbreviations.

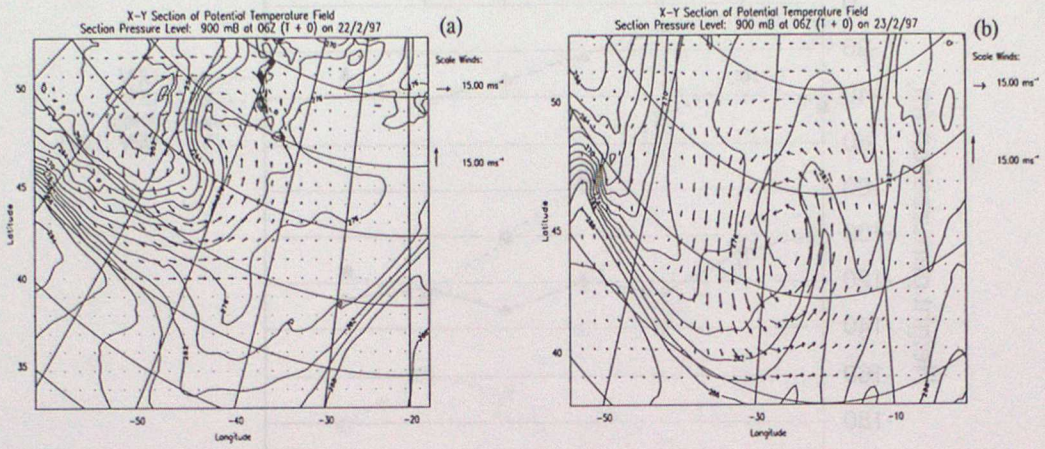

Figure 9. Winds at 900 mb induced by the UPV anomaly (vectors) overlaid with potential temperature on that level (solid lines, 3 K contour interval) for (a) 0600 UTC 22 February and (b) 0600 UTC 23 February 1997.

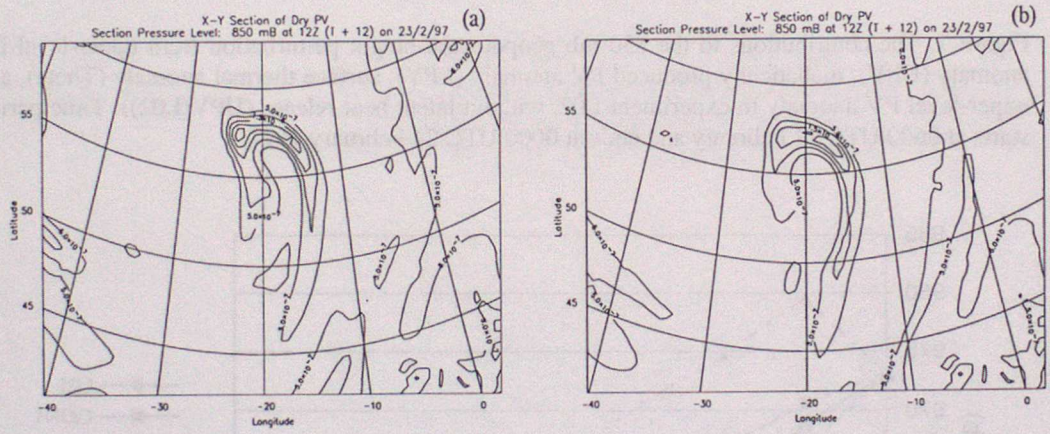

Figure 10. 850-mb PV (contour interval 0.5 PVU) for (a) CON1 and (b) MLP experiments at 1200 UTC 23 February, 12h after the start of the integration.

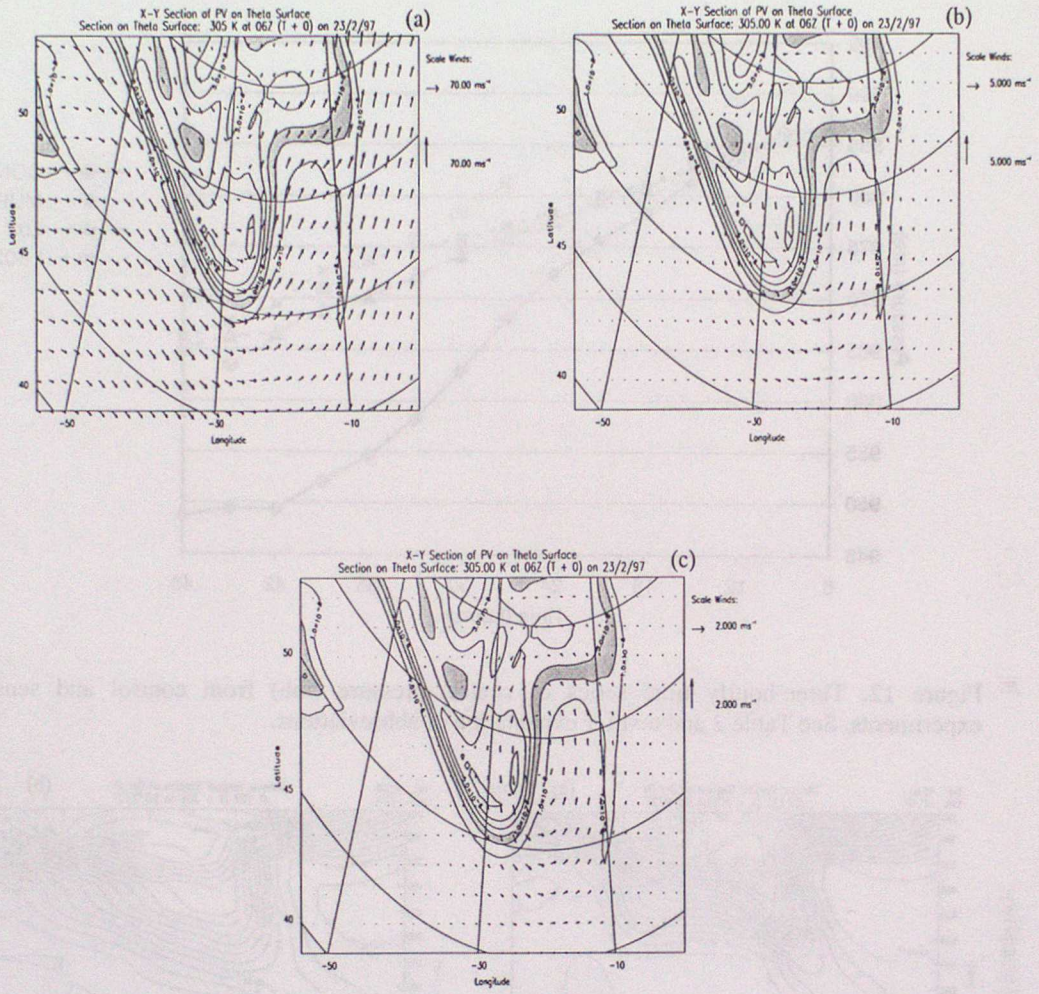

Figure 11. PV field on the 305 K isentropic surface at 0600 UTC 23 February with wind vectors overlaid: (a) original winds, (b) winds induced by the LPV anomaly, and (c) winds induced by the θ_B anomaly. PV contour interval is 1 unit, with values between 2 and 3 shaded. Note the different wind vector scales at upper right.

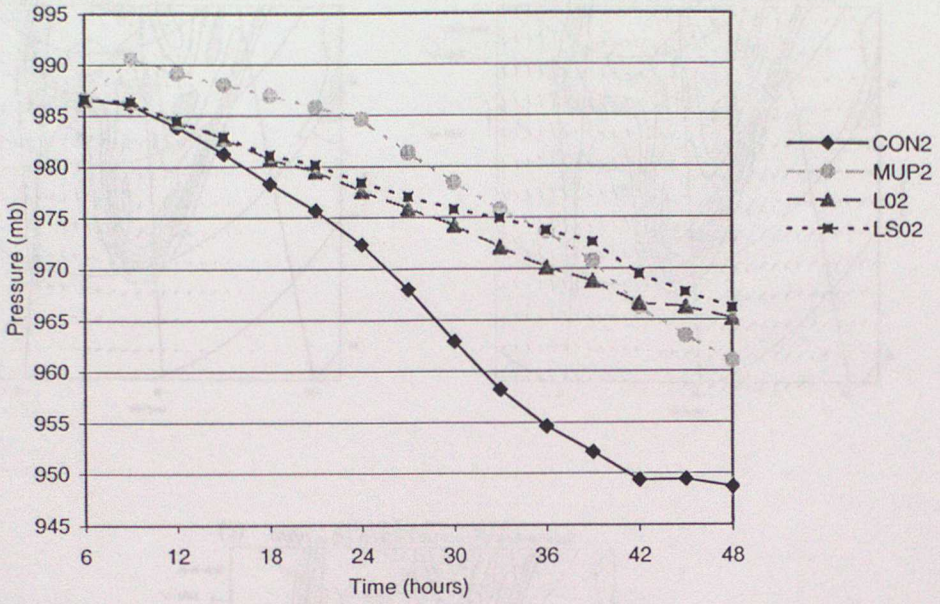

Figure 12. Three-hourly time series of central pressure (mb) from control and sensitivity experiments. See Table 2 and text for explanation of abbreviations.

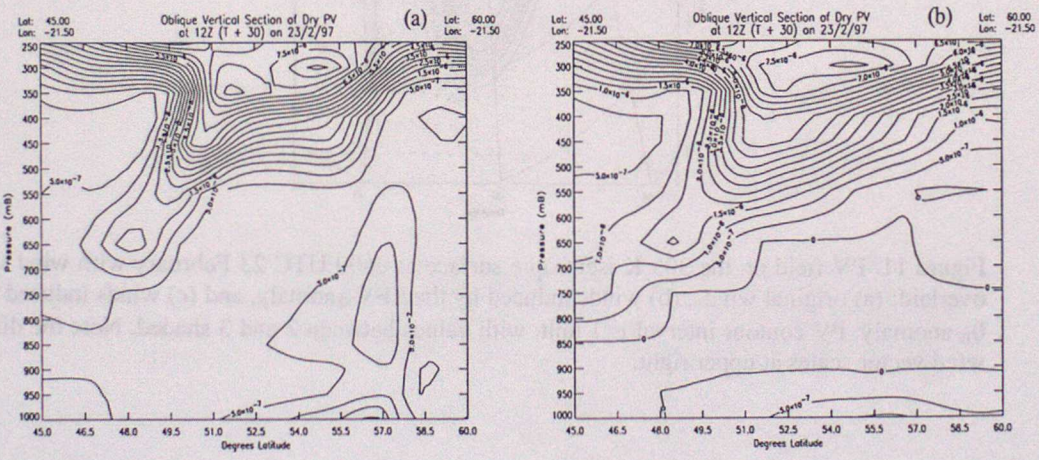

Figure 13. North – south cross sections of PV at 1200 UTC 23 February 1997; (a) CON2 and (b) L02 experiments. Contour interval is 0.5 PVU.

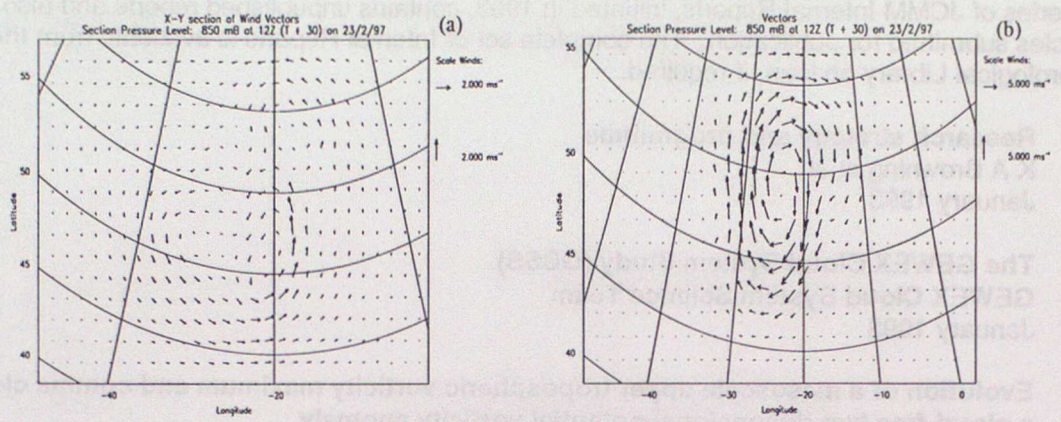

Figure 14. Change in 850-mb winds associated with UPV anomaly at 1200 UTC 23 February when (a) downstream ridge aloft excluded, and (b) all effects of latent heat release excluded. Vector scales in m s^{-1} are shown at upper right.

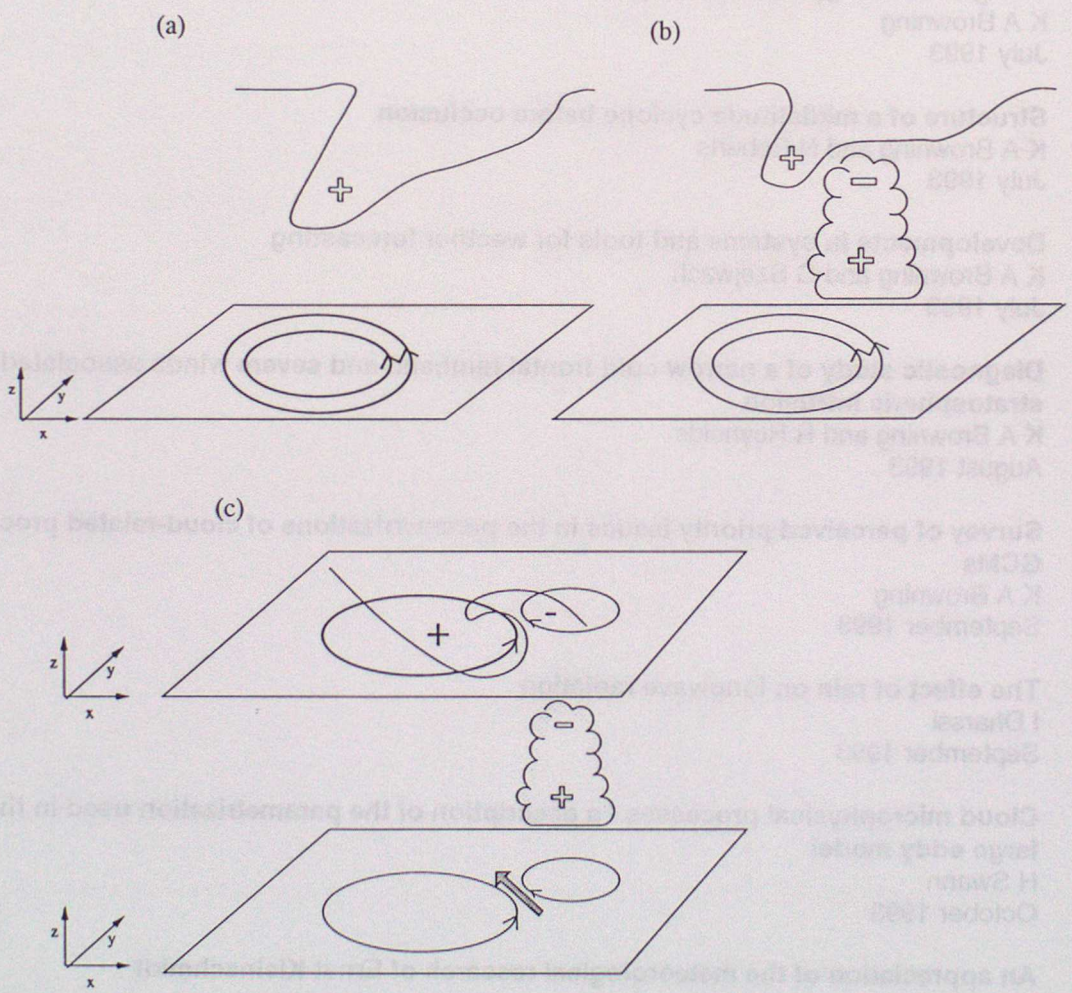

Figure 15. Schematic illustration of the various effects of latent heat release on the low-level circulation associated with the UPV anomaly; (a) with no latent heat release, (b) the negative effect, and (c) the positive effect. See text for explanation.